Title

Catestatin selects for the colonization of antimicrobial-resistant gut bacterial communities

Authors

Pamela González-Dávila [1#], Markus Schwalbe [1#], Arpit Danewalia [2], Boushra Dalile [3], Kristin Verbeke[3], Sushil K Mahata [2,4$], Sahar El Aidy [1$]

Affiliations

[1] Host-Microbe Metabolic Interactions, Groningen Biomolecular Sciences and Biotechnology Institute (GBB), University of Groningen, Groningen, the Netherlands

[2] Department of Medicine, University of California San Diego, La Jolla, CA, USA.

[3] Translational Research in GastroIntestinal Disorders (TARGID), Department of chronic diseases and metabolism, Faculty of Medicine, KU Leuven, Leuven, Belgium

[4] VA San Diego Healthcare System, San Diego, CA, USA.

[#] Shared first author

[$] Shared correspondence: Sushil K Mahata, smahata@health.ucsd.edu

Sahar El Aidy, sahar.elaidy@rug.nl

Abstract

The gut microbiota is in continuous interaction with the innermost layer of the gut, namely the epithelium. One of the various functions of the gut epithelium, is to keep the microbes at bay to avoid overstimulation of the underlying mucosa immune cells. To do so, the gut epithelia secrete a variety of antimicrobial peptides, such as chromogranin A (CgA) peptide catestatin (CST: $hCgA_{352-372}$). As a defense mechanism, gut microbes have evolved antimicrobial resistance mechanisms to counteract the killing effect of the secreted peptides. To this end, we treated wild-type mice and CST knockout (CST-KO) mice (where only the 63 nucleotides encoding CST have been deleted) with CST for 15 consecutive days. CST treatment was associated with a shift in the diversity and composition of the microbiota in the CST-KO mice. This effect was less prominent in WT mice. Levels of the microbiota-produced short-chain fatty acids, in particular, butyrate and acetate were significantly increased in CST-treated CST-KO mice but not the WT group. Both CST-treated CST-KO and WT mice showed a significant increase in microbiota-harboring phosphoethanolamine transferase-encoding genes, which facilitate their antimicrobial resistance. Finally, we show that CST was degraded by *Escherichia coli* via an omptin-protease and that the abundance of this gene was significantly higher in metagenomic datasets collected from patients with Crohn's disease but not with ulcerative colitis. Overall, this study illustrates how the endogenous antimicrobial peptide, CST, shapes the microbiota composition in the gut and primes further research to uncover the role of bacterial resistance to CST in disease states such as inflammatory bowel disease.

Keywords

Antimicrobial peptide; microbiota; resistance; phosphoethanolamine transferase; omptin

57

58 **Introduction**

59 The complex microbial community inhabiting the mammalian gut, and in particular their
60 metabolic products, has a crucial effect on various health and disease states, such as
61 inflammatory bowel disorders [1]. Gut microbiota, and its products, are in continuous interaction
62 with the innermost layer of the gut, namely the gut epithelium. Part of the gut epithelial function
63 is to keep the microbes at bay to avoid overstimulation of the underlying immune cells in the
64 gut, and the subsequent inflammation [2,3]. To do so, the gut epithelial cells secrete a wide variety
65 of antimicrobial peptides.

66 CST, a proteolytically processed product of Chromogranin-A (CgA), acts as an antimicrobial
67 peptide [4,5]. The pro-protein CgA is abundantly expressed in endocrine and neuroendocrine cells
68 including the epithelial enteroendocrine cells (EECs) [6–9]. CST consists of 21 amino acid residues
69 and acts on a wide range of regulatory functions including immune, endocrine, metabolic,
70 neurological, and cardiovascular functions [10–14]. For example, mice with a selective deletion of
71 the CST-coding region of the *Chga* gene (CST-KO mice) displayed increased gut permeability,
72 which was restored by CST treatment [15].

73 To date, a few studies have indicated associations between CST and the gut microbiota.
74 Intrarectal administration of CST for 6 days, in mice, resulted in a shift in the gut microbiota
75 composition, with a decrease of *Firmicutes* and an increase in the *Bacteroidota* phyla (Rabbi,
76 Munyaka, and Eissa 2017). These findings suggest the role of CST as a modulator of the gut
77 microbiota composition. This CST-modulatory effect could be mediated by its antimicrobial
78 activity against a wide range of microorganisms. In fact, CST has been reported to have
79 antimicrobial activity against pathogenic bacteria and filamentous fungi in *in-vitro* studies, [5]. In
80 humans, CST showed antimicrobial effects against several skin microbes [16]. Nevertheless, the
81 underlying mechanisms by which CST exerts its effects *in vivo* on the gut microbiota remain
82 obscure. In this study, we show how CST plays a role in governing the colonization of the gut
83 microbiota.

84

Results

Catestatin treatment affects the microbiota composition in CST-KO and WT mice.

The composition of the gut microbiota is shaped by, among others, host-produced antimicrobial peptides [17,18]. Here, we treated CST-KO and WT mice (n=12) with 2 µg/g body weight/day CST by intraperitoneal injection for 15 consecutive days. Amplicon sequencing of the V3-V4 regions of the bacterial 16S rRNA gene was performed on the fecal samples of CST-KO and WT mice with and without CST treatment (n=12). Microbial richness, assessed by the number of observed amplicon sequence variants (ASVs) and ACE index (Abundance-based Coverage Estimator), showed a significant decrease in CST-KO compared to WT mice **(Figure 1A)**. In contrast, the richness levels were restored upon treatment of CST-KO mice, but not in WT mice treated with CST. Next, the microbiota diversity was determined by Shannon's *H* and inverted Simpson's index, both indices are used to measure similar parameters of alpha diversity. Similar to the richness scores, the diversity index was significantly higher in the CST-treated CST-KO mice but not in the CST-treated WT group **(Figure 1B).** The data highlight that the effect of the absence of CST in CST-KO mice on the microbiota diversity and richness could be restored upon treatment with CST, while in WT mice, with normal CST levels in their gut, the microbiota diversity and richness did not change with CST treatment.

As a general exploratory analysis, principal component analysis (PCA) was performed and showed distinct clustering of the CST-KO, WT, and CST-treated groups **(Supplementary Figure 1A)**. Particularly, the CST-KO group clustered away from the other 3 groups, while the cluster of CST-treated WT mice showed a great spread and was overlapping with clusters of CST-treated CST-KO mice and WT mice.

To correct for any residual variation in the data, we further employed constrained RDA (redundancy analysis) to determine which bacterial taxa were associated with the different groups of mice at the genus level. The analysis was constrained to both, the mouse genotype and treatment (non-treated and CST-treated). Similar to the cluster separation detected by PCA analysis **(Supplementary Figure 1A)**, both constraints had a significant influence on the model ($p < 0.001$, determined by ANOVA-like permutation test), explaining 13.4% (genotype) and

113 9.8% (treatment) of the variation, respectively (**Figure 1C**). Notably, the CST treated CST-KO
114 group was shifted to the left side along RDA1, indicating a shift in "genotype" upon CST
115 treatment, as opposed to WT, where the treatment group only moved along RDA2, which is
116 associated with the treatment.
117 To assess the treatment effect exclusively on each genotype, we performed RDA constrained to
118 untreated and CST-treated groups. On the genus level, *Dubosiella* and *Romboutsia* showed the
119 strongest association with CST treatment along RDA1 (explaining ~31.2% of the variation) in the
120 CST-KO mice (**Supplementary Figure 1B**). In WT mice, RDA demonstrated an association of
121 *Faecalibaculum, Bifidobacterium, Romboutsia,* and *Anaeroplasma* with the baseline along RDA1
122 (~17.2% explained variance), while *Akkermansia* was more associated with PC1 (~25.1%
123 explained variance; residual variance). *Alloprevotella* and *Candidatus Saccharimonas*
124 representing the strongest associations with CST treatment in WT (**Supplementary Figure 1B**).
125 To further identify which bacterial taxa were affected by the CST treatment, pairwise
126 comparisons of bacterial abundances were performed between CST-treated and untreated groups
127 for each genotype. Focusing on the phylum level, Firmicutes decreased in relative abundance,
128 while Bacteroidota*,* Patescibacteria*,* Desulfobacterota, and Proteobacteria increased with CST
129 treatment in both CST-KO and WT groups. Verrucomicrobiota showed lower abundance in CST-
130 KO but increased significantly in CST-treated groups **(Figure 1D).** The changes depicted on the
131 phyla level in CST-treated WT mice are consistent with findings from Rabbi et al, albeit different
132 CST administration and dosage regimen [19]. These shifts in the main bacterial phyla upon CST
133 treatment was further confirmed to be consistent in human microbiota by *in vitro* culturing of
134 healthy human fecal samples with 10 μM CST **(Supplementary Figure 1C).** On family level the
135 most prominent changes were observed for Erysipelotrichaceae, which was consistently
136 decreased in treated groups and Lachnospiraceae, which was increased in CST-KO, but
137 decreased in WT in the CST treated groups. Further Lactobacillaceae was found to be decreased
138 in CST-KO, but increased in WT CST treated groups **(Figure 1D)**. On the genus level, CST
139 treatment reduced the abundance of *Staphylococcus* and *Turicibacter* in CST-KO and WT mice,
140 while *Alistipes, Akkermansia, and Roseburia,* were significantly increased only in the CST-KO

141 group (**Supplementary Excel Sheet**). Next, we used LEfSe (Linear discriminant analysis Effect
142 Size; Segata et al., 2011) to complement our differential abundance analysis. The main
143 discriminant feature separating the groups (untreated and CST-treated) in CST-KO mice were
144 species from the genera *Atopostipes, Jeotgalicoccus*, *Turicibacter*, *Staphylococcus*, and
145 Coriobacteriaceae *UCG-002* family **(Figure 1E)**. In WT mice, the most discriminating genera
146 were *Lactobacillus*, *Candidatus Sacchararimonas*, *Turicibacter*, and *Enterococcus*.
147 Changes in microbial composition are often accompanied by metabolic changes, in particular, the
148 production of short-chain fatty acids (SCFAs) [20]. Thus, levels of SCFAs; acetate, butyrate, and
149 propionate, were measured in the cecum of untreated and CST-treated CST-KO and WT mice
150 **(Figure 1F)**. CST treatment significantly increased the levels of acetate and butyrate in CST-KO
151 mice but not in the WT group. Specifically, butyrate was significantly lower in the CST-KO mice
152 compared to their WT counterparts. Both observations are consistent with the observed
153 significant increase in the SCFA-producing bacteria, *Alistipes*, *Akkermansia*, and *Roseburia* in the
154 CST-KO group.
155 Overall, the results indicated a significant impact of CST treatment on the diversity and
156 composition of the microbiota in the CST-KO mice, where CST is absent. This effect was much
157 less prominent in WT mice, which have normal levels of CST.
158
159 **CST treatment of CST-KO mice promotes the growth of core taxa present in WT mice.**
160 To investigate whether certain taxa exhibit similar behavior (increase or decrease in abundance)
161 between genotypes when CST is administered, we focused on the core microbiota (common taxa
162 between CST-treated groups), representing microbiota members, which directly (e.g., via
163 resistance genes) or indirectly (e.g., via cross-feeding), resist the antimicrobial effect of CST. To
164 do so, log-fold changes between CST treated and untreated groups for both WT and CST-KO
165 mice were compared **(Figure 2)**. Almost all significant changes in core taxa (determined by
166 unpaired Wilcoxon test) were exclusively higher in abundance in CST treated CST-KO mice
167 (quadrants I and II), while, for WT, both significant increases and decreases in the abundance of
168 core taxa were observed. These results coincide with the RDA analysis (cluster of CST-treated

169 CST-KO group moving closer to WT) and indicate that the effect of CST treatment in CST-KO
170 mice promotes the growth of core taxa associated with WT mice. Taxa present in quadrant II,
171 which represent those common taxa between the untreated WT and treated CST-KO mice, are
172 partially restored in their abundance in the latter group. Of note is, that *Turicibacter* was the only
173 core taxon in both genotypes, exclusively negatively affected by CST treatment, exhibiting a
174 significant decrease in abundance and therefore suggesting higher susceptibility to CST. To
175 confirm this observation, we performed *in vitro* assays, to determine minimum inhibitory
176 concentrations (MIC) for *Turicibacter sanguinis*. MIC was also performed for *Bacteroides*
177 *thetaiotaomicron*, which increased in abundance upon CST treatment. The screening revealed
178 low MIC for *T. sanguinis* (32 μM CST)*,* while *B. thetaiotaomicron* had a higher MIC (>64 μM
179 CST), thus confirming our *in vivo* observations. Reverse-phase HPLC analysis of spent culture
180 supernatant after 24 hrincubation with CST revealed degradation/uptake of CST from the
181 medium, in the case of *B. thetaiotaomicron,* but seemingly less for *T. sanguinis*, hence explaining
182 the higher MIC value in *B. thetaiotaomicron* (**Supplementary Figure 2**). Taken together, the
183 data imply that the changes in the gut microbiota composition associated with the CST treatment
184 **(Figure 1)** may be caused by the antimicrobial resistance of certain taxa to CST. However, the
185 underlying mechanisms remain obscure.
186
187 **Catestatin treatment promotes the abundance of the gut microbiota harboring**
188 **antimicrobial resistance phosphoethanolamine transferase-encoding genes.**
189 To determine whether bacteria with an increase in abundance in CST-treated groups harbor
190 antimicrobial resistance genes, a metagenomic prediction was performed using PiCRUSt2 on KO
191 (KEGG Orthology) level. From a panel of known AMP resistance genes [21], one KEGG Orthologue
192 (K03760) was found to be significantly different in abundance between CST treated and
193 untreated WT mice and close to significance in CST-KO, when corrected for multiple testing
194 (**Supplementary Excel Sheet**).
195 Sequences within this KEGG Orthogroup contain orthologs of EptA (*E. coli*) phosphoethanolamine
196 transferase. As KEGG Orthologs only contain sequences from reference genomes with no specific

197 gut metagenomic context, we sought to refine our search to investigate the taxonomical
198 distribution of the EptA. To do so, the EptA protein sequence from *E. coli* BW25113 was used as
199 a query to search the mouse gastrointestinal bacterial catalog (MGBC). Identified protein
200 sequences were further filtered and a phylogenetic tree was constructed, which exhibited a
201 distinct grouping of sequences without great dispersion and most of the sequences of the same
202 phylum were clustered in separate clades. This showed a major subdivision between of the
203 foremost sequences from Bacteroidota, Proteobacteria and Campylobacterota **(Figure 3A)**.
204 Using the taxonomical distribution of *eptA,* we reanalyzed the abundance of genera harboring
205 *eptA* upon CST treatment. Here, both CST-treated groups showed a significant increase in
206 microbiota-harboring *eptA*, though the effect in the CST-KO group seemed to be more
207 pronounced **(Figure 3B)**. To further support our findings that *eptA*-harboring core taxa increase
208 in abundance in CST treated groups, we looked at individual log-fold changes of single taxa, as
209 described above **(Figure 2)**. Indeed, *eptA*-harboring core taxa were higher in abundance in CST
210 treated groups, regardless of the genotype **(Supplement Figure 3A)**.
211 To further confirm the bioinformatics analysis outcome for the involvement of the *eptA* gene in
212 CST resistance, wild-type *E. coli* BW25113 and an *eptA* knockout strain (*ΔeptA*) were employed
213 and were cultured in different concentrations (8-100 μM) of CST **(Figure 3C).** The results
214 indicate that the lack of *eptA* led to a decreased carrying capacity at higher CST concentrations
215 **(Figure 3C)**, which is equivalent to the maximum population size of the culture, as well as a
216 concentration-dependent prolonged lag-phase during the growth of the *E. coli* **(Figure 3C).**
217 Similar to the majority of known antimicrobial peptides, CST is recognized by the PhoPQ system,
218 which involves the induction of expression of the gene *pmrD*, followed by activation of *pmrA,* and
219 eventually *eptA* expression [23]. To this end, we tested the expression of the above-mentioned
220 transcription regulators in *E. coli* BW25113 strain. Most notably, *phoP* showed approximately 3-
221 fold increase at 0.5 h after stimulation of *E. coli* BW25113 strain stimulated with 20 μM CST
222 (sufficient concentration for detection without growth penalty), but only 2-fold and less
223 prolonged in the control, before returning to baseline expression. The *pmrA* showed a later
224 upregulation (after 1h) compared to *phoP* in *E. coli* BW25113 CST-stimulated cultures, while

225 *pmrD* expression spiked in the presence of CST, but was invariant between the different
226 conditions (**Supplementary Figure 3B**).
227 Taken together, the results show a higher abundance of the bacteria-harbouring *eptA*-like genes
228 upon CST treatment, potentially providing these CST-resistant bacteria an advantage to colonize
229 the gut and, in turn, indirectly affect the colonization of other bacterial taxa.
230

231 **Catestatin peptide is degraded by *E. coli* omptin protease**

232 The ability of *E. coli* BW25113$^{\Delta eptA}$ to still resist comparatively high CST concentrations lead us to
233 test whether the bacterium harbours an additional resistance mechanism, such as degradation or
234 uptake, similar to what we observed in *B. thetaiotaomicron* **(Figure 3D)**. We analyzed the spent
235 culture supernatant by reverse-phase HPLC, which showed absence of CST-corresponding peaks
236 after 24 h of incubation with *E. coli* BW25113$^{\Delta eptA}$ as well as *E. coli* BW25113 **(Supplementary**
237 **Figure 4A)**. To test whether the enzyme involved in the CST degradation is excreted in the
238 supernatant, sterile-filtered supernatants of non-stimulated *E. coli* BW25113 cultures were
239 incubated with CST and subjected to tricine SDS-PAGE to visualize the degradation/uptake of
240 CST. Indeed CST was cleaved by *E. coli* BW25113 after incubation for different time intervals
241 from 30 min up till 24 h **(Figure 4A)**. This suggested the involvement of a secreted or
242 membrane-anchored protease, which can also be present in secreted vesicles, in CST
243 degradation. To identify which protease was involved, literature search was performed and
244 revealed that *E. coli* harbours only 2 major outer membrane proteases, predicted to cleave CST
245 [24]. Among those proteases is the omptin, an outer membrane protease, encoded by *ompT*. To
246 confirm that omptin was responsible for the CST degradation, an *E. coli ompT* knockout strain (*E.*
247 *coli* BW25113$^{\Delta ompT}$) was employed and was cultured in different concentrations of CST. Compared
248 to the wild-type and *E. coli* BW25113$^{\Delta eptA}$ strains, *E. coli* BW25113$^{\Delta ompT}$ showed no growth at 100
249 μM CST and an extensively prolonged lag-phase at 64 μM (**Figure 3D and Figure 4B)**.
250 Collectively, the results imply that wild-type *E. coli* BW25113 possesses the ability to cleave CST
251 through its outer membrane protease omptin, providing the bacterium with another defense
252 mechanism, together with EptA, to resist the antimicrobial action of CST.

253 To further confirm the complementary function of EptA and omptin, we performed qPCR on
254 control (unstimulated) and CST-stimulated cultures of wild-type *E. coli* BW25113 and *E. coli*
255 BW25113$^{\Delta ompT}$. The expression of *eptA* was upregulated about 1.7-fold in *E. coli* BW25113$^{\Delta ompT}$
256 without CST stimulation compared to the wild-type strain (**Figure 4C**). When stimulated with 20
257 μM CST, an increase in the expression of *ompT,* but not *eptA*, was detected *in* wild-type *E. coli*
258 BW25113 without stimulation and at 0.5 h after stimulation, while this effect was reversed at
259 later time points (**Supplementary Figure 3B**).
260 As *E. coli* BW25113 is considered a lab-strain, which might not be representative of naturally
261 occurring *E. coli* strains, we also tested for the presence of *ompT* in two gut isolate strains,
262 namely *E. coli* Nissle 1917 and *E. coli* DSM 11250. Both were found to be *ompT* carrying
263 (**Supplementary Figure 4B**). Taken together, the results indicate the capacity of *E. coli* strains
264 harbouring omptin to degrade CST, plausibly altering endogenous levels of the peptide in the gut
265 in cases where the abundance of *E. coli* is significantly increased, such as in inflammatory bowel
266 disease [25] To test this hypothesis, we investigated the abundance of *ompT*-like genes (KO term
267 K01355) in different subtypes of inflammatory bowel diseases (IBD), which are also associated
268 with altered levels of CST [15], using publicly available data from the MetaQuery database [26]. A
269 significant increase in the abundance of *ompT*-like genes was found between non-IBD and
270 Crohn's disease patients. Similarly, there was a significant increase in the abundance of *ompT*-
271 like genes between Crohn's disease patients and patients with ulcerative colitis, but not between
272 ulcerative colitis diseased and non-IBD subjects (**Figure 4D**). This observation was consistent
273 with the abundance of *E. coli* in those patients (**Figure 4D**). Overall, the data indicate that CST
274 degradation by bacteria-harbouring omptin-like proteases may play a role in altered levels of the
275 peptide previously detected in IBD patients, which in turn would result in an overgrowth of these
276 bacteria and worsening of the disease situation.
277

278 **Discussion**

279 This study unravels the crucial role of CST on the microbiota composition in the fecal samples of
280 WT and CST-KO mice. Specifically, there was a significant increase in the abundance of taxa that
281 harbor the CST peptide-resistance enzyme, phosphoethanolamine transferase in CST-KO and WT
282 mice treated with CST **(Figure 3B).** The shifts observed in the microbial phyla in this study after
283 treating WT mice with CST are in agreement with the findings of Rabbi *et al.,* who also reported
284 an increase in *Bacteroidota* and a decrease in *Firmicutes*, albeit a different route for the
285 administration of CST and dosage [19]. Low abundance of Bacteroidota, especially
286 *Bacteroides*/*Prevotella* have been linked to obesity, and CST-KO mice were described to be
287 insulin resistant and obese besides having elevated blood pressure [13,27]. In contrast, increased
288 *Bacteroidetes/Firmicutes* ratio has been associated with IBD [28,29], which is also characterized by
289 elevated levels of CST [15]. Nevertheless, as CST is a multifunctional peptide, acting directly on the
290 microbiota as well as on the host, any changes related to CST treatment should be viewed as a
291 complex interplay and not direct causation originating from the microbiota [12].

292 CST treatment could, only to a small extent, restore the microbial composition in a CST-depleted
293 environment, to the composition detected in an environment already primed with CST (WT mice)
294 **(Figure 2)**. In general, the effect of CST treatment observed in the CST-KO group was
295 significantly greater than that in the WT group **(Figure 1)**. This difference could be attributed to
296 the presence of normal levels of CST in the WT mice; thus, the microbiota is already primed with
297 the peptide and has evolved mechanisms to resist its antimicrobial effect. In contrast, the CST-
298 KO group, in which CST is absent, may harbor bacteria that are susceptible to the CST
299 antimicrobial activity but were eradicated upon CST treatment **(Figure 2)**. Especially the core
300 taxa resisting CST treatment seem to benefit from their presence in the gut lumen environment,
301 by exhibiting an increase in abundance. Introduction of CST to a CST-depleted environment did
302 not necessarily promote exclusively health beneficial microbiota, but rather led to a more
303 equilibrated composition, including also pathobiont taxa. For example, in CST-treated CST-KO,
304 *Oscillibacter* and *Mucispirillum* **(Figure 2)**, both of which increased in relative abundance, have
305 been found to increase in diet-induced obesity and might be considered as pathobionts [30,31].

306 Similarly, *Alistipes* was shown to have a detrimental influence on colorectal cancer progression,
307 despite contrasting evidence that it also has protective effects against colitis or cardiovascular
308 diseases [32]. On the other side *Odoribacter*, a SCFA-producer, which increased in relative
309 abundance in CST-treated WT mice **(Figure 2)** has been linked to immunomodulatory effects
310 and general health benefits presumably also in cooperation with *Akkermansia* [33].
311 So far, antimicrobial resistance mechanisms have been mostly investigated in pathogens due to
312 their implication on antibiotic resistance. In *in-vitro* studies, CST has been reported to have an
313 inhibitory effect against the pathogenic gram-positive (*Micrococcus luteus*, *Bacillus megaterium*),
314 gram-negative bacteria (*Escherichia coli* D22), and filamentous fungi (*Neurospora crassa and*
315 *Aspergillus fumigatus)* [5]. Moreover, human CST showed antimicrobial effects against several skin
316 microbes including the gram-positive (*Staphylococcus aureus* and Group A *Streptococcus*),
317 gram-negative bacteria (*E. coli* O29*,* and *Pseudomonas aeruginosa*), also (*Candida albicans)*, and
318 filamentous fungi (*Aspergillus niger, Aspergillus fumigatus, Trichophyton rubrum*) [16].
319 As a defense mechanism, bacteria have evolved several systems to survive the effect of the
320 antimicrobial peptides [21]. The ability to withstand these peptides provides a potential benefit in
321 colonization over other members of the gut microbiota especially under pathological conditions
322 [34]. Analogously, antimicrobial peptides are regularly used by the host to select for specific gut
323 microbiota in homeostatic situations. For CST, the antimicrobial activity resides in the N-terminal
324 of the peptide, which is highly cationic [5]. These positive charges in the peptide interact with the
325 anionic components of the bacterial cell membrane, resulting in the permeabilization of microbial
326 membranes, leading to cell lysis [7]. The present study suggests that CST may as well play a role
327 in aiding the host to select for which microbes to colonize the gut. The abundance of bacteria
328 encoding the phosphoethanolamine transferase genes increased upon CST treatment **(Figure**
329 **3A-E)**. This is not surprising since the *E.coli* phosphoethanolamine transferase e*ptA*, for
330 example, has been linked to colistin resistance, being a cyclic proteinogenic antibiotic [35]. EptA
331 acts by modifying core lipopolysaccharide components with ethanolamine, increasing membrane
332 charge and thus, repelling the antimicrobial agent. The fact that EptA-like proteins are abundant
333 across a variety of different taxa present in the human gastrointestinal tract **(Figure 3A-C)**

334 implies that antimicrobial resistance is a mutualistic and important component in the selection of
335 a specific microbiota composition by the host, through active modulation of antimicrobial peptide
336 levels, such as CST. Indeed, this paradigm is supported by our findings that CST treatment
337 induced a large-scale alteration in the microbiota composition not only in the CST-KO group but
338 also in the WT group, both of which clustered closer to each other, and further away from the
339 untreated groups **(Figure 1)**.
340 The induced expression of *eptA* gene in *E. coli* BW25113$^{\Delta ompT}$ **(Figure 4C)** implies a
341 complementary mechanism when other defense mechanisms are missing. Indeed, we uncovered
342 the degradation of CST by wild-type *E. coli*, a member of the gut microbiota via omptin, an outer
343 membrane protease, known to cleave other cationic antimicrobial peptides, such as protamine or
344 LL-37 [36,37]. The presence of these fragments with high proteolytic activity in the gut has its
345 implications on the microbiota composition, as it may facilitate colonization of other CST-
346 susceptible bacteria [38]. It remains elusive though, whether CST is taken up and accumulating
347 inside the bacteria or is further degraded, and what the fate of the resulting cleavage fragments
348 is, e.g., through uptake by other microbiota or interaction with the host. Analogously it remains
349 unclear how other bacteria, such as *B.thetathiomicron* can degrade CST **(Supplementary**
350 **figure 2)** and how widespread such a phenomenon is among the gut bacteria.
351 Levels of CST are increased in IBD patients, while *E. coli* was associated with the development
352 and progression of different IBD types [25,39]. The higher abundance of *ompT*-like genes in samples
353 from Crohn's disease patients, which coincided with a higher abundance of *E.coli* **(Figure 4D)**,
354 suggests that bacteria harboring *ompT*-like genes, such as *E. coli,* may have a benefit to colonize
355 the gut due to its ability to resist CST. In cases where the overall microbial composition is
356 compromised, and the endogenous levels of CST are altered, like in IBD, such bacterial
357 resistance may cause particular bacterial strains to be involved in worsening the gut
358 inflammation. Overgrowth of gut bacteria with the capacity to resist CST may lead the host to
359 secrete higher levels of CST as a defense mechanism. The levels of CST were reported to be
360 higher in IBD patients compared to healthy subjects [15]. It remains unclear why only samples
361 from Crohn's disease patients but not ulcerative colitis showed a higher abundance of *ompT* as

362 well as *E. coli.* One plausible explanation could be due to the different *E. coli* strains
363 predominantly present in either Crohn's disease or ulcerative colitis [25] **(Figure 4D)**.
364 Overall, the present study highlights the significant role of the CST peptide in determining the
365 microbiota composition. The fact that gut bacteria with a capacity to resist the antimicrobial
366 effect of CST become more abundant upon CST treatment, suggests that these bacteria may
367 have gained an advantage over other microbiota members to survive the gut environment,
368 which, indirectly shapes the colonization of the total community. Further studies should also
369 explore the changes elicited by CST administration on host physiology, which might in turn affect
370 the gut microbiota composition. One limitation of the present study is the relatively uncontrolled
371 actual concentrations of CST that eventually reach the gut after intraperitoneal injection. This
372 concentration variability could increase interindividual variability in the microbial composition.
373
374
375

376 **Materials and Methods**

377 **Animals**

378 All studies with mice were approved by the University of California San Diego (UCSD) and
379 Veteran Affairs San Diego Healthcare System (VASDHS) Institutional Animal Care and Use
380 Committees for the Mahata laboratory (UCSD: #S00048M; VA: #A13-002) and were performed
381 in San Diego in adherence to the NIH Guide for the Care and Use of Laboratory Animals. Our
382 experiment was based on a single cohort of mice which constisted of twelve mice per group each
383 (control and CST-treatment, per genotype); out of those, twenty four male adult C57BL/6 J mice
384 (age 20 weeks) were purchased from Jackson Laboratory (Bar Harbor, ME) and twenty four
385 CST-KO mice (age 20-28 weeks) generated in the Mahata laboratory, were used. CST-KO mice
386 have a deletion in the 63 bp CST domain from Exon VII of the *Chga* gene [27] in C57BL/6
387 background. Mice from WT and CST-KO groups were injected intraperitoneally once daily with
388 CST (2 μg/g body weight; Genscript Biotech Corporation, Piscataway, NJ) for 15 days based on
389 previous experimentation [15]. Mice were housed in 4 to 5 animals per cage and had free access to
390 water and food (Normal Chow Diet, LabDiet 5001) in temperature and humidity-controlled rooms
391 with a 12-hr light/dark cycle.

392

393 **Determination of short-chain fatty acids (SCFAs) in cecal samples**

394 Cecal samples (100 mg) were suspended in 1 mL of saturated NaCl (36%) solution. An internal
395 standard (50 μL of 10.7 μM 2-methyl butyric acid in MQ water) was added and the samples were
396 homogenized using glass beads. After the addition of 150 μL H_2SO_4 96%, SCFAs were extracted
397 with 3 ml of ether. The ether layer was collected and dried with Na_2SO_4 (150 mg). The
398 supernatant (0.5 μL) was analyzed using gas chromatography with flame ionization detection
399 (Agilent, Santa Clara, California, USA). The system was equipped with a DB FFAP analytical
400 column (30m x 0.53 mm ID, 1.0 μm; Agilent) and helium GC grade (5.6) was used as carrier gas
401 with a constant flow of 4.2 ml/min. The initial oven temperature was held at 100 °C for 3 min,
402 ramped with 4 °C/min to 140 °C (isothermal for 5 min) and further with 40 °C/min to 235 °C

403 (isothermal for 15 min). The resulting chromatograms were processed using ChemStation
404 (Agilent Technologies).
405
406 **DNA isolation and 16S rRNA gene sequencing**
407 DNA isolation was performed on fecal samples that were collected from untreated and CST-
408 treated WT and CST-KO mice. A phenol-chloroform-isoamyl alcohol procedure was used for DNA
409 extraction [40]. Briefly, the pellet was resuspended in 1 ml of lysis buffer (940 µl TE buffer, 50 µl
410 SDS 10% and 10 µl Proteinase K 20 mg/ml) in a 2 ml screw cap micro-tube containing a mix of
411 zirconium and glass beads. Then, samples were incubated at 58 °C for 1 hour and 150 µl of
412 buffered phenol (Invitrogen, 15513-047) was added. To support lysis, samples were
413 homogenized 3 × 30 sec with 1-min intervals on ice in a mini bead-beater (Biospec, Bartlesville,
414 USA). This was followed by the addition of 150 µl chloroform/isoamyl alcohol (24:1) and
415 centrifugation at 16,000x *g* for 10 min and 4 °C. The upper layer was carefully transferred to a
416 clean tube, 300 µl of phenol-chloroform-isoamyl alcohol [25:24:1] was added, centrifuged and
417 the process was repeated by adding 300 µl of chloroform-isoamyl alcohol [24:1]. To precipitate
418 the DNA, the upper layer was transferred to a new tube and 1 volume of absolute isopropanol
419 and 1/10 volume of 3 M sodium acetate was added. Samples were incubated overnight at -20
420 °C. Subsequently, samples were centrifuged at 16,000x *g* for 20 min at 4 °C, the supernatant
421 was discarded and the pellet was washed with 700 µl of 70% ethanol. After ethanol aspiration
422 the DNA pellet was air-dried for 30 min and resuspended in 100 µl TE buffer. In each step,
423 samples were vigorously mixed using a vortex.
424 Sequencing of the V3-V4 region of the bacterial 16S rRNA gene was carried out by Novogene Co.
425 Ltd. Briefly, for sequencing library preparation, raw DNA extracts were diluted to 1 ng/µl in
426 sterile water, and amplicons were generated by PCR (primers 341F and 806R) using a Phusion
427 High-Fidelity PCR Master Mix (New England Biolabs). Amplification product quality was assessed
428 by gel electrophoreses and samples were pooled in equimolar ratios. Libraries were generated
429 with a NEBNext Ultra DNA Library Prep Kit for Illumina and sequencing was carried out on an

430 Illumina MiSeq 250 bp paired-end platform. Initial processing of reads involved trimming of
431 adapters and primers using a Novogene in-house pipeline (Novogene Co. Ltd, Cambridge, UK).
432

433 **Microbiota analysis**

434 Paired-end sequencing reads were filtered, denoised, merged, and classified with the *dada2*
435 package in the statistical programming language R while processing forward and reverse reads
436 separately until merge [41,42]. Briefly, reads were truncated to 220 bases and low-quality reads
437 were filtered followed by dereplication. Error models were learned, while manually enforcing the
438 monotonicity of the error function. Reads were denoised and merged with minimal overlap of 12
439 bp, while non-merging reads were concatenated. Singletons have been removed before
440 performing bimera removal, followed by read classification using SILVA (V138) as a taxonomical
441 reference database.

442 For downstream analysis, the *phyloseq* and *microbiome* packages were used, samples were
443 rarefied to even depth and richness was determined by the number of observed amplicon
444 sequence variants (ASVs), as well as ACE index and alpha diversity was assessed via Shannon's
445 *H* and inverted Simpson indexes [43,44]. All ASVs were collapsed on genus level and cumulative
446 sum scaling was applied using *metagenomeSeq* [45]. The resulting genus abundance table served
447 as input for different types of ordinations such as principal component analysis (PCA) or
448 redundancy analysis (RDA). The significance of constraints in constrained RDA was determined
449 by permutation-like ANOVA. Differential abundance was assessed by unpaired Wilcoxon Rank
450 Sum test using $p < 0.05$ as a significance threshold followed by FDR correction.

451 To generate the double log-fold change plot, first, the core microbiota were estimated for each
452 group by filtering raw ASV counts to contain only more than 10 reads and be present in more
453 than 10% of the samples. Next, only taxa intersecting between CST treated groups were
454 selected and analyzed further. Differential abundance was assessed by a Wilcoxon Rank Sum
455 test between treated and untreated groups per genotype and FDR corrected. Only taxa with an
456 adjusted $p < 0.05$ were considered further. Their mean log-fold changes between groups were
457 calculated and plotted against each other.

458 Further LefSe analysis was carried out, adjusting the alpha value for factorial Kruskal-Wallis test
459 and the alpha value for pairwise Wilcoxon tests to 0.01. Additionally, the LDA score threshold
460 was set to 3.0 [46]
461 For the functional analysis, the metagenomic prediction from 16S rRNA gene sequencing data
462 was done using PiCRUSt2, using raw ASVs and unnormalized ASV abundances [47]. For this, ASVs
463 were first filtered to have a minimal abundance of 10 reads and to be present in at least 1/10 of
464 the samples. PiCRUSt2 was run with standard parameters and stratification enabled. The
465 metagenomic data was further analyzed by using STAMP v2.1.3 [48]. For statistical analysis,
466 White's non-parametric t-test, two-sided, and Benjamini-Hochberg multiple test correction were
467 used to reveal differences between groups.
468
469 **Phylogenetic analysis**
470 The amino acid sequence of the *E. coli eptA* gene (UniProt P30845) was searched with *phmmer*
471 from the hmmer suite (v3.3.1; hmmer.org) against a non-redundant dataset of the mouse
472 gastrointestinal bacterial catalog (MGBC) [49]. Hits were filtered on full sequence E-value,
473 excluding all sequences with an E-value greater than 0.5x the median absolute deviation from
474 the median. Additionally, only sequences originating from genomes with >90% completeness
475 and <1 contamination were taken into account. Sequences were dereplicated, aligned with
476 MAFFT (v7.453) and a phylogenetic tree was constructed using FastTree (v2.1.11) [50,51]. The
477 produced gene tree was visualized with FigTree (v1.4.4), to aid visibility the tree was pruned
478 using Treemmer (v0.3; with parameter -RTL 0.95) [52]
479
480 **Bacteria and growth inhibition assay**
481 *E. coli* BW25113, BW25113$^{\Delta ompT}$ (JW0554) and BW25113$^{\Delta eptA}$ (JW5730) (**Supplementary Table**
482 **1**) were routinely grown aerobically in Difco Antibiotic Medium 3 (BD, Franklin Lakes, USA) at 37
483 °C degrees without agitation. Bacteria were inoculated from −80 °C stocks and grown overnight.
484 Before the experiment, cultures were diluted at 1:100 in fresh medium from overnight cultures.
485 Five different CST concentrations were tested in triplicates in a 96-well plate. For this, 10 µl of a

486 10x concentrated stock of CST were added to 90µl of diluted culture to obtain final
487 concentrations of 8, 16, 32, 64, and 100 µM. Bacterial growth was monitored for 24 h at 600 nm
488 (OD600) with shaking for 5s every 15 min using a BioTek ELx808 microplate reader (BioTek,
489 Winooski, USA). Growth curves were fit using the *growthcurver* R package (v0.3.0).
490

491 **Tricine SDS-PAGE**

492 Overnight cultures of *E. coli* strains BW25113 and BW25113$^{\Delta ompT}$ **(Supplementary Table x)**
493 were centrifuged at 10,000 g for 10 min at 4°C and the supernatant was collected. The
494 supernatant was further sterile filtered (0.2 µm filters) and to 90 µl of supernatant 10 µl of a 10x
495 CST stock was added to reach a final concentration of 100 µM. Aliquots of 20 µl were taken at
496 time points 0.5, 4, and 24 h.
497 To visualize CST degradation, culture supernatants were run on Tricine SDS-PAGE following a
498 modified protocol [53]. Briefly, gels consisted out of a 4% stacking gel and a 16% resolving gel
499 both with a cross-linker ratio of 19:1, and were prepared to standard procedure. For sample
500 prep, 10 µl of each sample were mixed with 10 ml of reducing sample buffer (100 mM Tris-HCl,
501 1% SDS, 4% 2-mercaptoethanol, 0.02% Coomassie Brilliant Blue, 24% glycerol) and incubated
502 at 70°C for 5 min. Subsequently, 10 µl of the sample was loaded on the gel, first, run for ~30
503 min at 30 V, and then at 170 V for 90 min. Silver staining was applied to visualize proteins using
504 various modifications in fixation to avoid loss of small proteins [54]. For this, gels were fixed (30%
505 ethanol, 15% formalin, 5% acetic acid) for 60 min and quickly washed once with 50% ethanol
506 and twice with MilliQ-filtered water. Gels were incubated for 40 min in 0.005% sodium
507 thiosulfate, followed by incubation for 40 min in 0.1% silver nitrate solution containing 0.07%
508 formalin. Washing with MilliQ-filtered water was performed and a 2% sodium carbonate solution
509 containing 0.1% formalin was added. Gels were incubated for 1-2 min until bands became visible
510 and development was stopped by removing the developer and adding 50 mM EDTA solution. Gels
511 were then imaged in a ChemiDoc MP Imaging System (BioRad, Hercules, USA).
512

513 **Expression analysis**

514 Overnight cultures of *E. coli* BW25113, *E. coli* BW25113$^{\Delta eptA}$, and *E. coli* BW25113$^{\Delta ompT}$ were
515 resuspended 1:1000 in 6 ml of fresh Difco Antibiotic Medium 3 and grown until OD600 0.5 was
516 reached. Aliquots of 1 ml were harvested, centrifuged at 10,000 g for 10 min, and immediately
517 stored at -80 °C. This and all subsequent centrifugation steps were done at 4 °C.

518 For culture stimulation with CST *E. coli* BW25113 or *E. coli* BW25113$^{\Delta ompT}$ was resuspended
519 1:1000 in 6 ml fresh Difco Antibiotic Medium 3 and grown until OD600 0.5. An aliquot of 5 ml
520 was harvested and centrifuged at 3,000 g for 10 min. The pellet was resuspended in fresh
521 medium containing 20 µM CST and gently mixed. Samples of 1 ml were taken at time points 0h
522 (before resuspension), 0.5h, 1h, 2h, and 4h, subsequently centrifuged at 10,000 g for 10 min
523 and immediately stored at -80 °C.

524 RNA was isolated using a phenol:chloroform:isoamyl alcohol procedure as previously described
525 [55]. The harvested bacterial pellet was resuspended in 200 µl TE buffer and transferred to a tube
526 containing 0.5 g of 0.1 mm zirconia/silica beads, 25 µl 10% SDS, and 200 µl
527 phenol:chloroform:isoamyl alcohol solution. The subsequent procedure was performed as
528 described and isolates were stored at -80°C until further use.

529 qPCR was carried out according to standard procedures [56]. Briefly, 2 µg of RNA were reverse
530 transcribed using a High-Capacity cDNA Reverse Transcription Kit with RNAse Inhibitor (Applied
531 Biosystems, Vilnius, Lithuania). Subsequently, 10 ng of cDNA were used for qPCR employing a
532 PowerUp SYBR Green Master Mix (Applied Biosystems, Vilnius, Lithuania) and primers for genes
533 *eptA, ompT, phoP, pmrD, pmrA* and *tus*. Reactions were performed in a clear 96-well plate using
534 a CFX96 Real-Time PCR System (BioRad, Hercules, USA). Gene expression was assessed by
535 normalizing to housekeeping gene *tus* using the R package *qpcR* (v1.4) for curve fitting and the
536 *pcr* (v1.2.2) package for differential expression calculation employing the $2^{-\Delta\Delta Ct}$ method as
537 described in [57].

538

539 **Statistical analysis**

540 All statistical tests were performed using GraphPad Prism 7 or the statistical programming
541 language R. Specific statistical tests are indicated in the text or figure legends. Normality was
542 assessed by either D'Augustino-Pearson omnibus normality test or Shapiro-Wilk normality test. If
543 normality was met a t-test was chosen, otherwise non-parametric Mann-Whitney was used.
544 Outliers were assessed with GraphPads ROUT method (Q=1).
545
546 **Data availability statement**
547 All data generated or analyzed during this study are included in this manuscript and its
548 supplementary information files. The 16S rRNA gene amplicon sequence data were deposited
549 under BioProject number PRJNA741992.
550
551 **Authors' Contributions**
552 P.G-D., M.S, S.E.A and S.K.M conceived and designed the study. P.G-D., M.S., B.D, and S.K.M.
553 performed the experiments, and P.G-D., M.S, B.D., and S.E.A analyzed the data. P.G-D, M.S,
554 S.E.A. wrote the original manuscript that was reviewed by A.D, B.D., K.V., and S.K.M. Funding
555 for these studies were acquired by S.E.A. and S.K.M. All authors read and approved the final
556 manuscript.
557
558 **Acknowledgment**
559 P.G-D thanks the National Council of Science and Technology in Mexico (CONACyt) for the Ph.D.
560 grant assigned to CVU 690069. We thank Dr. Matthias Heinemann of Department of Molecular
561 Systems Biology, University of Groningen, the Netherlands, for providing us *ΔeptA* and *ΔompT E.*
562 *coli* BW25113 mutant strain; Dr. Greet Vandermeulen of Department of chronic diseases and
563 metabolism, Faculty of Medicine, KU Leuven, Belgium for the help with SCFAs analysis.
564
565 **Funding**

S.E.A is supported by a Rosalind Franklin Fellowship, co-funded by the European Union and the University of Groningen, The Netherlands. S.K.M. is supported by a Merit Review Grant (I01 BX003934) from the Department of Veterans Affairs, USA.

Conflict of interest

The authors declare no competing interests.

573 **References**

574 1. Kåhrström CT, Pariente N, Weiss U. Intestinal microbiota in health and disease.
575 Nature. 2016 Jul 7;535(7610):47–47.

576 2. El Aidy S, van Baarlen P, Derrien M, Lindenbergh-Kortleve DJ, Hooiveld G, Levenez F,
577 et al. Temporal and spatial interplay of microbiota and intestinal mucosa drive
578 establishment of immune homeostasis in conventionalized mice. Mucosal Immunol.
579 2012;5(5):567–79.

580 3. Okumura R, Takeda K. Roles of intestinal epithelial cells in the maintenance of gut
581 homeostasis. Exp Mol Med. 2017 May 26;49(5):e338–e338.

582 4. Mahata SK, O'Connor DT, Mahata M, Yoo SH, Taupenot L, Wu H, et al. Novel
583 autocrine feedback control of catecholamine release. A discrete chromogranin a
584 fragment is a noncompetitive nicotinic cholinergic antagonist. J Clin Invest. 1997 Sep
585 15;100(6):1623–33.

586 5. Briolat J, Wu SD, Mahata SK, Gonthier B, Bagnard D, Chasserot-Golaz S, et al. New
587 antimicrobial activity for the catecholamine release-inhibitory peptide from
588 chromogranin A. Cell Mol Life Sci. 2005 Feb;62(3):377–85.

589 6. Lugardon K, Raffner R, Goumon Y, Corti A, Delmas A, Bulet P, et al. Antibacterial and
590 antifungal activities of vasostatin-1, the N-terminal fragment of chromogranin A. J
591 Biol Chem. 2000;275(15):10745–53.

592 7. Aslam R, Atindehou M, Lavaux T, Haïkel Y, Schneider F, Metz-Boutigue M-H.
593 Chromogranin A-Derived Peptides Are Involved in Innate Immunity. Curr Med Chem.
594 2012;19(24):4115–23.

595 8. El-Salhy M, Patcharatrakul T, Hatlebakk JG, Hausken T, Gilja OH, Gonlachanvit S.
596 Chromogranin A cell density in the large intestine of Asian and European patients with

597 irritable bowel syndrome. Scand J Gastroenterol. 2017 Jun-Jul;52(6-7):691-697.

598 9. Bartolomucci A, Possenti R, Mahata SK, Fischer-Colbrie R, Loh YP, Salton SR. The
599 extended granin family: structure, function, and biomedical implications. Endocr Rev.
600 2011 Dec;32(6):755-97

601 10. Mahata SK, Corti A. Chromogranin A and its fragments in cardiovascular,
602 immunometabolic, and cancer regulation. Ann N Y Acad Sci. 2019 Nov 6;1455(1):34–
603 58.

604 11. Corti A, Marcucci F, Bachetti T. Circulating chromogranin A and its fragments as
605 diagnostic and prognostic disease markers. Pflugers Archiv European Journal of
606 Physiology. 2018.

607 12. Mahata SK, Mahata M, Fung MM, O'Connor DT. Catestatin: A multifunctional peptide
608 from chromogranin A. Regul Pept. 2010 Jun;162(1–3):33–43.

609 13. Ying W, Mahata S, Bandyopadhyay GK, Zhou Z, Wollam J, Vu J, et al. Catestatin
610 inhibits obesity-induced macrophage infiltration and inflammation in the liver and
611 suppresses hepatic glucose production, leading to improved insulin sensitivity.
612 Diabetes. 2018;67(5):841–8.

613 14. Mahata SK, Kiranmayi M, Mahapatra NR. Catestatin: A Master Regulator of
614 Cardiovascular Functions. Curr Med Chem. 2018 Apr 17;25(11):1352–74.

615 15. Muntjewerff EM, Tang K, Lutter L, Christoffersson G, Nicolasen MJT, Gao H, et al.
616 Chromogranin A regulates gut permeability via the antagonistic actions of its
617 proteolytic peptides. Acta Physiol. 2021 Jun 6;232(2).

618 16. Radek KA, Lopez-Garcia B, Hupe M, Niesman IR, Elias PM, Taupenot L, et al. The
619 neuroendocrine peptide catestatin is a cutaneous antimicrobial and induced in the
620 skin after injury. J Invest Dermatol. 2008;128(6):1525–34.

621 17. Bevins CL, Salzman NH. Paneth cells, antimicrobial peptides and maintenance of
622 intestinal homeostasis. Nat Rev Microbiol. 2011;9(5):356–68.

623 18. Dupont A, Heinbockel L, Brandenburg K, Hornef MW. Antimicrobial peptides and the
624 enteric mucus layer act in concert to protect the intestinal mucosa. Gut Microbes.
625 2014 Nov 2;5(6):761–5.

626 19. Rabbi MF, Munyaka PM, Eissa N, Metz-Boutigue MH, Khafipour E, Ghia JE. Human
627 catestatin alters gut microbiota composition in mice. Front Microbiol. 2017 Jan
628 17;7(JAN):1–12.

629 20. Tsukuda N, Yahagi K, Hara T, Watanabe Y, Matsumoto H, Mori H, et al. Key bacterial
630 taxa and metabolic pathways affecting gut short-chain fatty acid profiles in early life.
631 ISME J. 2021;15(9):2574–90.

632 21. Nuri R, Shprung T, Shai Y. Defensive remodeling: How bacterial surface properties
633 and biofilm formation promote resistance to antimicrobial peptides. Biochim Biophys
634 Acta - Biomembr. 2015;1848(11):3089–100.

635 22. Jakobsson HE, Rodríguez-Piñeiro AM, Schütte A, Ermund A, Boysen P, Bemark M, et
636 al. The composition of the gut microbiota shapes the colon mucus barrier. EMBO Rep.
637 2015;16(2):164–77.

638 23. Samantha A, Vrielink A. Lipid A Phosphoethanolamine Transferase: Regulation,
639 Structure and Immune Response. J Mol Biol. 2020;432(18):5184–96.

640 24. Gottesman S. Proteases and their targets in Escherichia coli. Annu Rev Genet.
641 1996;30:465–506.

642 25. Mirsepasi-Lauridsen HC, Vallance BA, Krogfelt KA, Petersen AM. *Escherichia coli*
643 Pathobionts Associated with Inflammatory Bowel Disease. Clin Microbiol Rev. 2019
644 Mar 20;32(2):1–16.

645 26. Nayfach S, Fischbach MA, Pollard KS. MetaQuery: A web server for rapid annotation
646 and quantitative analysis of specific genes in the human gut microbiome.
647 Bioinformatics. 2015;31(20):3368–70.

648 27. Ying W, Tang K, Avolio E, Schilling JM, Pasqua T, Liu MA, et al. Immunosuppression of
649 Macrophages Underlies the Cardioprotective Effects of CST (Catestatin).
650 Hypertension. 2021 May;77(5):1670–82.

651 28. Stojanov S, Berlec A, Štrukelj B. The influence of probiotics on the
652 firmicutes/bacteroidetes ratio in the treatment of obesity and inflammatory bowel
653 disease. Microorganisms. 2020;8(11):1–16.

654 29. Indiani CMDSP, Rizzardi KF, Castelo PM, Ferraz LFC, Darrieux M, Parisotto TM.
655 Childhood Obesity and Firmicutes/Bacteroidetes Ratio in the Gut Microbiota: A
656 Systematic Review. Child Obes. 2018;14(8):501–9.

657 30. Lam YY, Ha CWY, Campbell CR, Mitchell AJ, Dinudom A, Oscarsson J, et al. Increased
658 gut permeability and microbiota change associate with mesenteric fat inflammation
659 and metabolic dysfunction in diet-induced obese mice. PLoS One. 2012;7(3):1–10.

660 31. Herp S, Durai Raj AC, Salvado Silva M, Woelfel S, Stecher B. The human symbiont
661 *Mucispirillum schaedleri*: causality in health and disease. Med Microbiol Immunol.
662 2021;210(4):173–9.

663 32. Parker BJ, Wearsch PA, Veloo ACM, Rodriguez-Palacios A. The Genus Alistipes: Gut
664 Bacteria With Emerging Implications to Inflammation, Cancer, and Mental Health.
665 Front Immunol. 2020 Jun 9;11(June):1–15.

666 33. Hiippala K, Barreto G, Burrello C, Diaz-Basabe A, Suutarinen M, Kainulainen V, et al.
667 Novel *Odoribacter splanchnicus* Strain and Its Outer Membrane Vesicles Exert
668 Immunoregulatory Effects in vitro. Front Microbiol. 2020;11(November):1–14.

669 34. McPhee JB, Small CL, Reid-Yu SA, Brannon JR, Moual H Le, Coombes BK. Host
670 defense peptide resistance contributes to colonization and maximal intestinal
671 pathology by Crohn's disease-associated adherent-invasive Escherichia coli. Infect
672 Immun. 2014;82(8):3383–93.

673 35. Xu Y, Wei W, Lei S, Lin J, Srinivas S, Feng Y. An evolutionarily conserved mechanism
674 for intrinsic and transferable polymyxin resistance. MBio. 2018;9(2):1–18.

675 36. Thomassin JL, Brannon JR, Gibbs BF, Gruenheid S, Le Moual H. OmpT outer
676 membrane proteases of enterohemorrhagic and enteropathogenic *Escherichia coli*
677 contribute differently to the degradation of human LL-37. Infect Immun.
678 2012;80(2):483–92.

679 37. Desloges I, Taylor JA, Leclerc JM, Brannon JR, Portt A, Spencer JD, et al.
680 Identification and characterization of OmpT-like proteases in uropathogenic
681 *Escherichia coli* clinical isolates. Microbiologyopen. 2019;8(11):1–36.

682 38. Kulkarni HM, Nagaraj R, Jagannadham M V. Protective role of E. coli outer membrane
683 vesicles against antibiotics. Microbiol Res. 2015;181:1–7.

684 39. Muntjewerff EM, Dunkel G, Nicolasen MJT, Mahata SK, van den Bogaart G. Catestatin
685 as a Target for Treatment of Inflammatory Diseases. Front Immunol. 2018 Oct
686 4;9(OCT).

687 40. Santella RM. Approaches to DNA/RNA Extraction and Whole Genome Amplification:
688 Table 1. Cancer Epidemiol Biomarkers Prev. 2006 Sep;15(9):1585–7.

689 41. Callahan BJ, McMurdie PJ, Rosen MJ, Han AW, Johnson AJA, Holmes SP. DADA2:
690 High-resolution sample inference from Illumina amplicon data. Nat Methods.
691 2016;13(7):581–3.

692 42. R Core Team. R: A Language and Environment for Statistical Computing [Internet].

693 Vienna, Austria; 2019. Available from: https://www.r-project.org/

694 43. Lahti L, Shetty S. microbiome R package [Internet]. Available from:
695 http://microbiome.github.io

696 44. McMurdie PJ, Holmes S. Phyloseq: An R Package for Reproducible Interactive Analysis
697 and Graphics of Microbiome Census Data. PLoS One. 2013;8(4).

698 45. Paulson JN, Colin Stine O, Bravo HC, Pop M. Differential abundance analysis for
699 microbial marker-gene surveys. Nat Methods. 2013;10(12):1200–2.

700 46. Segata N, Izard J, Waldron L, Gevers D, Miropolsky L, Garrett WS, et al. Metagenomic
701 biomarker discovery and explanation. Genome Biol. 2011;12(6):R60.

702 47. Douglas GM, Maffei VJ, Zaneveld JR, Yurgel SN, Brown JR, Taylor CM, et al. PICRUSt2
703 for prediction of metagenome functions. Nat Biotechnol. 2020 Jun 1;38(6):685–8.

704 48. Parks DH, Tyson GW, Hugenholtz P, Beiko RG. STAMP: Statistical analysis of
705 taxonomic and functional profiles. Bioinformatics. 2014;30(21):3123–4.

706 49. Beresford-Jones BS, Forster SC, Stares MD, Notley G, Viciani E, Browne HP, et al. The
707 Mouse Gastrointestinal Bacteria Catalogue enables translation between the mouse
708 and human gut microbiotas via functional mapping. Cell Host Microbe.
709 2022;30(1):124-138.e8.

710 50. Katoh K, Standley DM. MAFFT multiple sequence alignment software version 7:
711 Improvements in performance and usability. Mol Biol Evol. 2013;30(4):772–80.

712 51. Price MN, Dehal PS, Arkin AP. FastTree 2 - Approximately maximum-likelihood trees
713 for large alignments. PLoS One. 2010;5(3):e9490.

714 52. Menardo F, Loiseau C, Brites D, Coscolla M, Gygli SM, Rutaihwa LK, et al. Treemmer:
715 A tool to reduce large phylogenetic datasets with minimal loss of diversity. BMC

716 Bioinformatics. 2018;19(1):1–8.

717 53. Haider SR, Reid HJ, Sharp BL. Tricine-SDS-PAGE. In: Kurien B., Scofield R. (eds)
718 Protein Electrophoresis. Methods in Molecular Biology (Methods and Protocols).
719 Totowa, NJ: Humana Press; 2012. p. 81–91.

720 54. Schägger H. Tricine-SDS-PAGE. Nat Protoc. 2006;1(1):16–22.

721 55. Zoetendal EG, Booijink CCGM, Klaassens ES, Heilig HGHJ, Kleerebezem M, Smidt H,
722 et al. Isolation of RNA from bacterial samples of the human gastrointestinal tract. Nat
723 Protoc. 2006;1(2):954–9.

724 56. Zhou K, Zhou L, Lim Q, Zou R, Stephanopoulos G, Too HP. Novel reference genes for
725 quantifying transcriptional responses of Escherichia coli to protein overexpression by
726 quantitative PCR. BMC Mol Biol. 2011;12(1):18.

727 57. Livak KJ, Schmittgen TD. Analysis of relative gene expression data using real-time
728 quantitative PCR and the 2-ΔΔCT method. Methods. 2001;25(4):402–8.

729

730

731 **Figures**

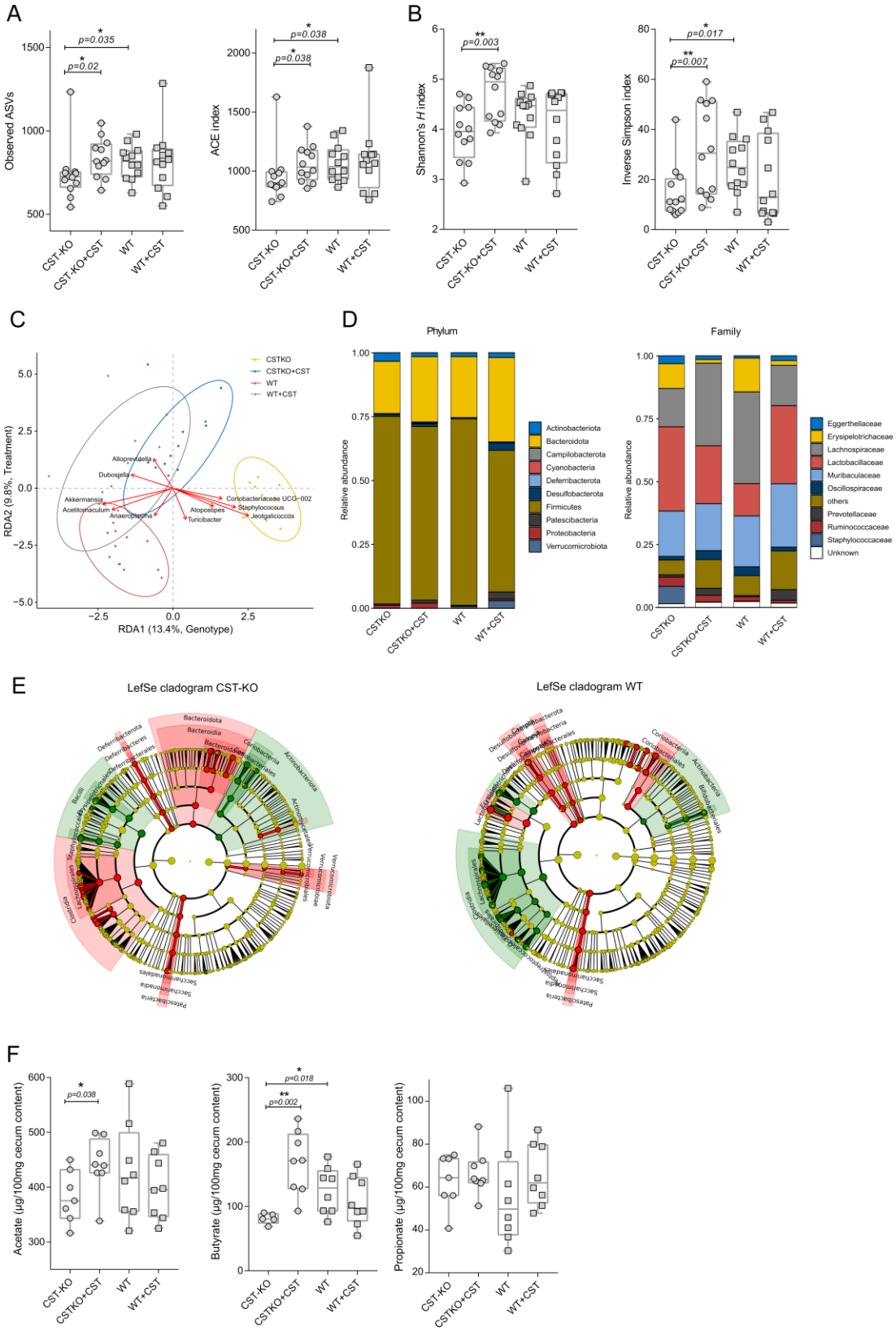

732

733 **Figure 1. CST treatment affects the murine fecal microbiota.** (**A, B**) Alpha diversity was
734 assessed using different metrics and is concordantly significantly increased upon CST treatment.
735 **(A)** represent the species richness (observed ASVs, ACE) and (**B**) species diversity of the CST-
736 KO and WT mice before and after CST treatment. Significance was tested with an unpaired
737 *Mann-Whitney* test. Boxes represent the median with interquartile range, and whiskers represent
738 the maxima and minima. (**C**) Genotype and treatment constrained redundancy analysis (RDA) on
739 genus collapsed abundances. Arrows indicate the association of taxa with samples, with the
740 length being a proxy for the strength of the association. Ellipses represent normal data
741 generated by the R package ggplot2. Significant separation of clusters and contribution of the
742 variables to the variance of the RDA was tested with Permutational Multivariate ANOVA
743 (PERMANOVA) and revealed significant ($p < 0.001$) effects of CST administration, both in CST-
744 KO and WT mice; grey – WT+CST, yellow – CST-KO, blue - CST-KO+CST. (**D**) Relative
745 abundance of the present phyla and families. (**E**) Cladograms of a LefSe analysis (Linear
746 discriminant analysis Effect Size) comparing microbiota changes upon CST treatment in CST-KO
747 and WT mice. Significance was tested using a Kruskal-Wallis (KW) test and Linear Discriminant
748 Analysis (LDA). A significant feature was considered when $p < 0.01$ and Log (LDA score) > 3.
749 The green color indicates the microbiota composition before CST treatment and the red color
750 after CST treatment. (**F**) Concentrations of cecal acetate, butyrate, and propionate, of CST-
751 treated (CST-KO, n=7; WT, n=8) and untreated animals (CST-KO, n=8; WT, n=8). Cecal acetate
752 and butyrate were significantly increased in CST-treated CST-KO mice. Boxes represent the
753 median with interquartile range, and whiskers represent the maxima and minima. Data were
754 analyzed using a 2-tailed paired *t*-test, while 2 outliers were removed using ROUT in GraphPad
755 Prism. Error bars are shown as mean ± SEM.
756
757

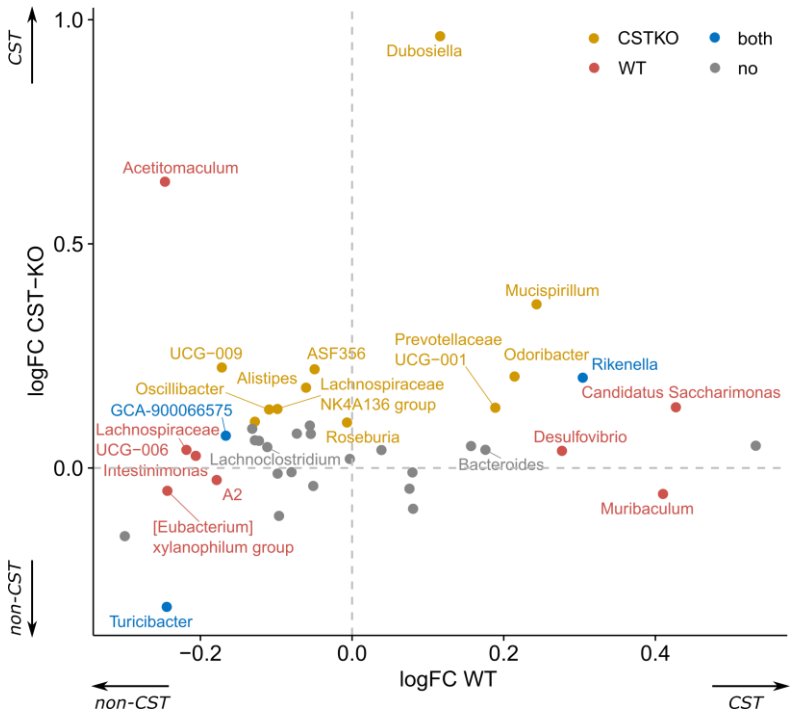

758

759 **Figure 2 Taxa able to endure CST treatment benefit from its presence in the**

760 **environment.** Scatter plot of log-fold changes, comparing abundance changes for significantly

761 abundant genera between treated and untreated groups per genotype. Colors represent

762 significance when testing for differential abundance between treated and untreated groups for

763 each genotype.

764

765

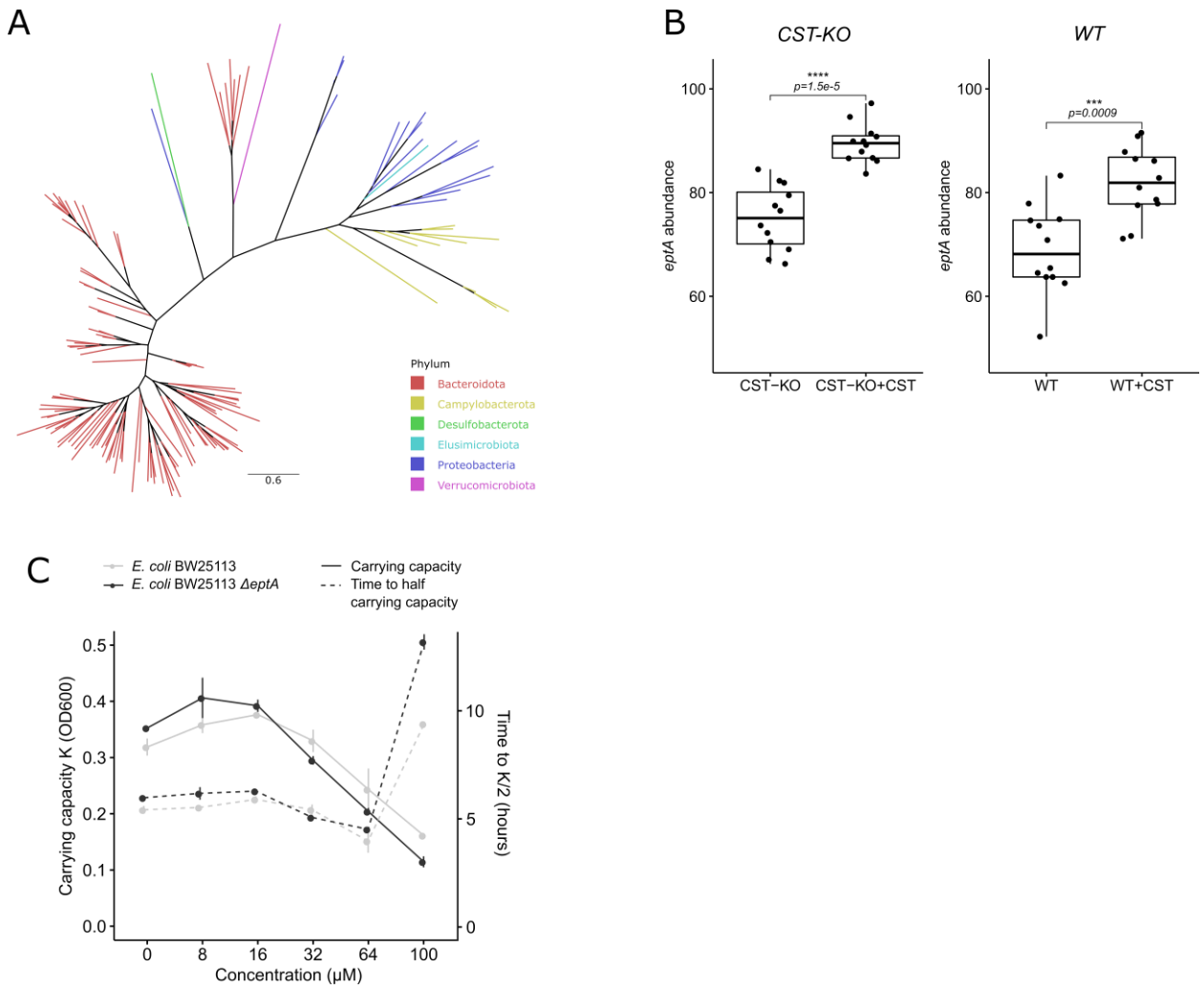

766

767 **Figure 3. CST treatment promotes the abundance of the antimicrobial resistance gene,**
768 ***eptA*.** (**A**) Unrooted phylogenetic tree depicting the distribution of orthologous *eptA*-like genes
769 throughout bacterial species in the mouse gut. The tree was pruned using Treemmer to aid
770 visualization, while branches were colored by the phylum they belong to. (**B**) Boxplot showing a
771 significant abundance increase of *eptA* harboring bacteria upon CST treatment, both in CST-KO
772 and WT mice. The *eptA* abundance is defined as the sum of abundances from all taxa harboring
773 an *eptA* gene. Boxes represent the median with interquartile range, and whiskers represent the
774 maxima and minima. Significance was assessed by an unpaired *t*-test. (**C**) CST inhibits the
775 growth of wild-type *E. coli* BW25113 and *E. coli* BW25113$^{\Delta eptA}$ strains, visualized by carrying
776 capacity K (a measure of maximum OD600) and time taken to reach half the carrying capacity

777 (inflection point of the growth curve at mid-log-phase) that depends on CST concentrations
778 ranging from 8-100 μM.
779
780

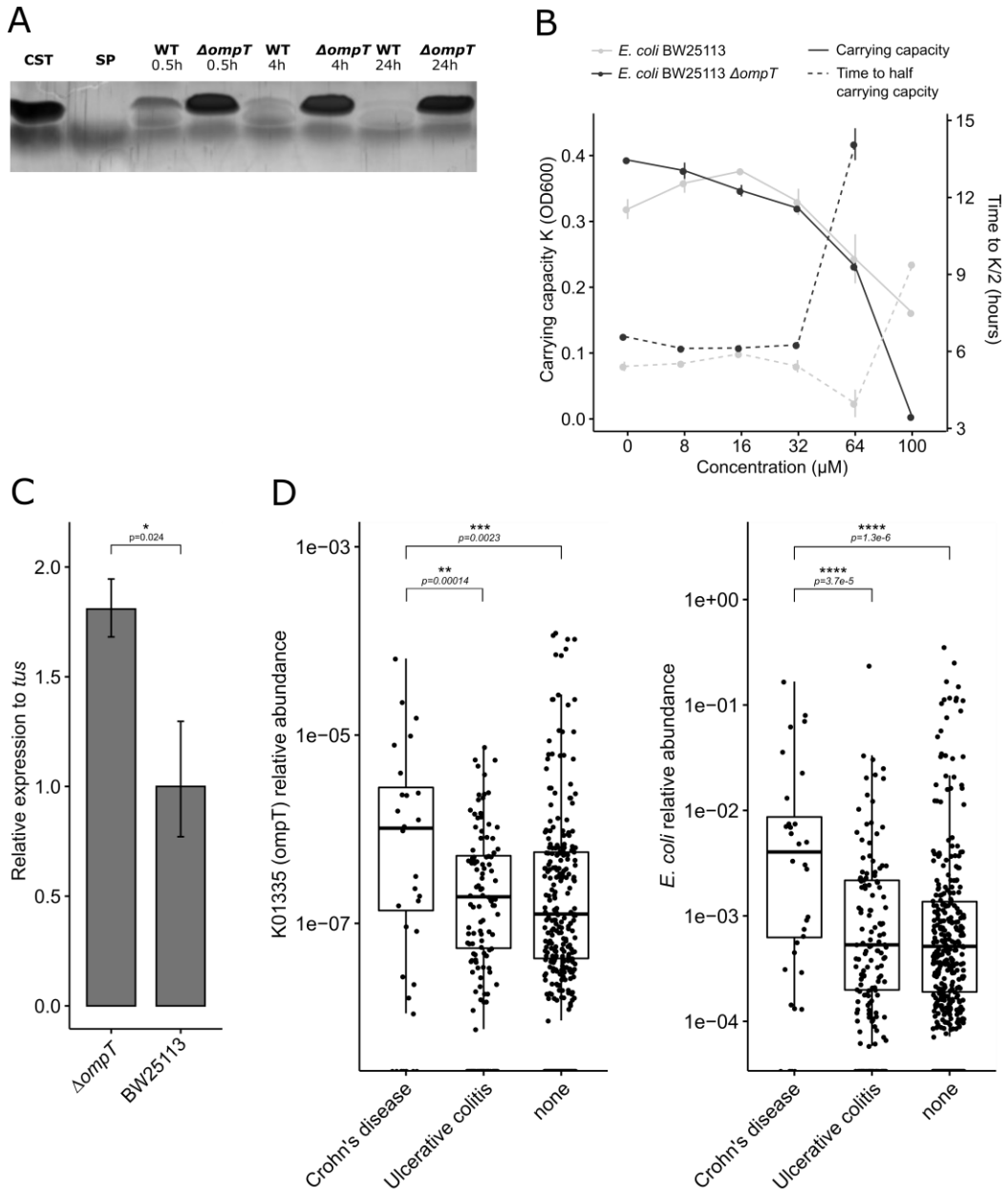

Figure 4. Omptin enzyme is responsible for the degradation of CST in *E coli*. (**A**) Silver-stained tricine SDS-PAGE gels showing the cleavage of CST by wild-type *E. coli* BW25113, but not in *E. coli* BW25113$^{\Delta ompT}$. Sterile non-stimulated culture supernatants were cultured with 100μM CST and samples were collected at different time points; CST: catestatin (2.3kDa), SP: substance P (1.3kDa) (**B**) CST inhibits the growth of *E. coli* BW25113$^{\Delta ompT}$, visualized by carrying capacity K (a measure of maximum OD600) and time taken to reach half the carrying capacity in CST concentrations ranging from 8-100 μM. (**C**) Baseline expression of *eptA* is increased in *E.*

789 *coli* BW25113$^{\Delta ompT}$ compared and normalized to that of wild-type *E. coli* BW25113. *tus* was used
790 as a housekeeping gene for normalization in both strains and statistical significance was
791 calculated using a Wilcoxon test. (**D**) Relative abundance of omptin like genes or *E. coli* in
792 patients with Crohn's disease, ulcerative colitis, and healthy subjects. Axes are on log10-scale
793 and significance was assessed using Wilcoxon test without stratification.
794